International Journal of Recent Technology and Engineering (IJRTE)
ISSN: 2277-3878 (Online), Volume-2 Issue-2, May 2013

Analysis of Residual Stresses and Distortions in Girth-Welded Carbon Steel Pipe

Prabhat Kumar Sinha, Raisul Islam, Chandan Prasad, Mohd. Kaleem

Abstract-*This article, the weld joint suffers various types of weld-induced residual stress fields (hoop and axial) and deformation patterns (axial shrinkage, radial shrinkage). In this paper Three-dimensional finite element modeling of residual stresses in a girth-welded carbon steel pipe is presented with an emphasis on modeling procedures for the global residual stress characteristics. To precisely capture the distortions and residual stresses, computational methodology based on three-dimensional finite element model for the simulation of gas tungsten arc welding in thin-walled pipe is presented. Butt-weld geometry with single "V" for a 300 mm outer diameter cylinder of 3 mm thick is used. The complex phenomenon of arc welding is numerically solved by sequentially coupled transient, non-linear thermo-mechanical analysis. The accuracy of both the thermal and structural models is validated through experiments for temperature distribution, residual stresses and distortion. The simulated result shows close correlation with the experimental measurements.*

Keywords: FEM; welding simulations; Distortions; Residual Stresses; Girth Weld.

I. INTRODUCTION

The distribution of residual stresses in a girth welded pipe is complex. Weld shrinkage in the circumferential direction induces both shearing and bending that result in stress components in the circumferential direction (hoop stress) and in the axial direction (meridian stress). Process and geometric related factors that influence residual stresses include welding heat input, pipe diameter, wall thickness and joint design [1-5].Brust, et al. [2], reported high tensile stresses in both axial and hoop directions on the pipe inner surface using the axisymmetric, inherent shrinkage model. However, discrepancies in stress magnitude were found between the predicted results and the experimentally measured data, particularly in the axial component in the outer surface.

Revised Manuscript Received on 30 May 2013.
* Correspondence Author
Prabhat Kumar Sinha, Mechanical Engineering Department Shepherd School of Engineering and Technology Sam Higginbottom Institute of Agriculture, Technology and Sciences (Formerly Allahabad Agriculture Institute) Allahabad 211007, India.
Raisul Islam, Mechanical Engineering Department Shepherd School of Engineering and Technology Sam Higginbottom Institute of Agriculture, Technology and Sciences (Formerly Allahabad Agriculture Institute) Allahabad 211007, India.
Chandan Prasad, Mechanical Engineering Department Shepherd School of Engineering and Technology Sam Higginbottom Institute of Agriculture, Technology and Sciences (Formerly Allahabad Agriculture Institute) Allahabad 211007, India.
Mohd. Kaleem, Mechanical Engineering Department Shepherd School of Engineering and Technology Sam Higginbottom Institute of Agriculture, Technology and Sciences (Formerly Allahabad Agriculture Institute) Allahabad 211007, India.

Numerical modelling using the finite element method (FEM) has been used by many researchers to predict weld residual stresses in complex welded structures.
To date, most of the finite element analysis[22] for pipe girth welds use the inherent shrinkage modelling technique that assumes an axisymmetric condition.
This is due to the fact that the three-dimensional, nonlinear FEM analysis of girth welds with a moving heat source is computational intensive and sometimes cost prohibitive. The inherent shrinkage model is incapable of predicting the transient residual stress distributions near the weld start and stop locations.
The complex nature of the welding process due to multi-field (thermal, mechanical, metallurgy etc.) interactions and intricate geometries in real world applications has made the prediction of weld-induced imperfections, a truly difficult and computationally intensive task. However, with the availability of 64 digit computers and refined FE tools, welding engineers around the world are more biased towards the computer simulations of complex welding phenomenon instead of the conventional trial and error approach on the shop floor. A significant simulation and experimental work focusing on circumferential welding is available in the literature [6-13]. As the computer simulation of welding processes is highly computationally intensive and large computer storage and CPU time are required, most of the previous research reduces computational power requirements by simplifying with assumptions such as rotational symmetry and lateral symmetry in numerical simulations [7-10]. These assumptions reduces the computational demand at the cost of the accuracy of the results because the model was over simplified by limiting the solution domain to only a section of the whole do-main with forced symmetry assumptions which did not prevails. Further, these simplified assumptions are not capable of capturing the considerable effects of weld start/stop and weld tack modeling. In this regard an experimental work by Jonsson and Josefson [16] and some three-dimensional finite element (FE) studies [12, 13, 15, 24]; reported deviations from rotational symmetry, especially at the beginning and end of the welding cycle for circumferential joint in welding of pipes with lateral symmetry. Later, by using a full three-dimensional model for multi-pass welding of pipes, Fricke et al. [16] concluded that residual stresses[21] are by no means axis-symmetric.
In the present analysis, the temperature fields and consequently the weld-induced residual stress fields and distortion patterns are investigated by numerical simulations based on FEM modeling. Tomodel the physics behind the gas tungsten arc welding (GTAW) process, a sequentially coupled,

Published By:
Blue Eyes Intelligence Engineering and Sciences Publication (BEIESP)

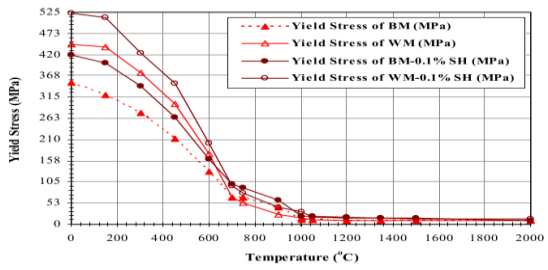

Legends : BM = Base Metal WM = Weld MetalSH = Strain Hardening

Fig. 1. Thermo-mechanical properties of low carbon steel as a function of temperature used in the present study.

Full 3D model is employed. Transient, non-linear thermal solution based on heat conduction, convective and radiative boundary conditions is solved in the first part to obtain the nodal temperature history. The temperature fields are further utilized as thermal loads in subsequent elastoplastic structural analysis to obtain the transient and residual stress fields and distortions.

II. FE ANALYSIS

2.1 FE model

For the girth weldingof two pipe with "V" groove [23], a full 3D FE model along with finite element statistics developed in ANSYS® is shown in Fig. 2. The element type in thermal analysis is SOLID70 (linear 8-node brick element with one degree of freedom, i.e., temperature at each node) and in structural analysis is SOLID45 (linear 8-node brick element with three degrees of freedom at each node: translations in the nodal x, y, and z directions.). Further details about the selected elements may be found in [17]. High temperature and flux gradients are anticipated in and around the fusion zone (FZ) and heat affected zone (HAZ); therefore, a relatively fine mesh is used within a distance of 10 mm on both sides of the weld line (WL). Away from the HAZ the element size increases with an increase in the distance from WL.In the weld direction, the element size is kept constant equal to 1.96 mm. Within the anticipated HAZ dimension of 10 mm on each side of the WLin transverse direction, the element size of 1 mm is used.
The element size away from the weld region increases with the increase in distance. In the thickness direction there are total three elements, 1 mm each to facilitate for “V” groove modeling.Two tack welds on the start, i.e., 0º and middle, i.e., 180º of the weld are modeled, each of which is comprised of 4 elements (7.85 mm) in circumferential direction and 4 and 2 elements (4mm and 2 mm, respectively) in two layers in thethickness direction. The used mesh is based on a mesh sensitivity analysis performed for successive mesh refinements.

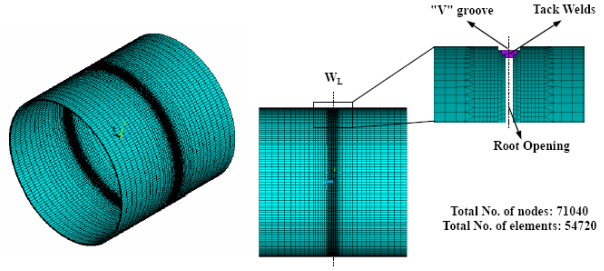

Fig. 2. (a) 3D FE mesh based on sensitivity analysis. (b) “V” groove, tack weld and root opening in FE model.

A number of thermal analyses based on the number of elements as indicated in Fig. 3 are conducted to see the corresponding effects of maximum temperature attained during the analysis. This maximum temperature attained is then considered as the basis for mesh refinement. As shown in Fig. 3, it is clear that no further increase in maximum temperature is achieved if the number of elements is increased beyond 54720. The mesh with number of elements indicated by the arrow in Fig. 3 is then considered for the analysis in order to get the mesh independent results. Tack lengths positions in the FE models are in accordance with the physical weld sample. Theoretically, two cylinders should be regarded as separate parts in the model setup, because they are independent until the moving heat source (welding torch) passes over and joins these together. Both the cylinders are modeled as a single model in FE modeling as the cylinders are tack welded to each other and mechanically restrained prior to welding.

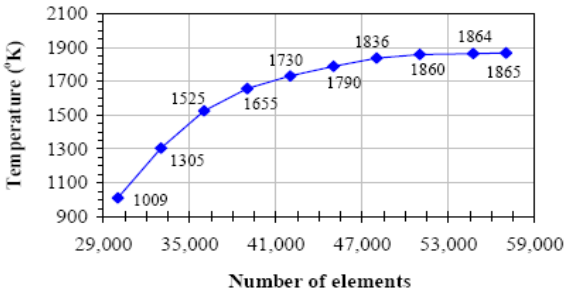

Fig. 3. Mesh sensitivity analysis based on maximum temperature attained.

2.2 Thermal analysis technique

A high non-uniform temperature field is generatedduring the welding process resulting in residual stresses in the welds. The transient temperature distribution is a function of total heat applied and heat distribution patterns within the domain and is highly sensitive to weldinduced residual stresses. A detailed and accurate thermal analysis with appropriate boundary conditions such as heat transfer by conduction, heat losses due to convection and radiation and heat input from the welding torch along with the effects of filler metal deposition, is of paramount importance for the determination of realistic temperature profiles. The governing equation for transient heat transfer analysis during welding process is given by Eq. (1).

$$\rho c \frac{\partial T}{\partial t}(x,y,z,t) = \nabla . q(x,y,z,t) + Q(x,y,z,t) \ldots\ldots(1)$$

where ρ is the density (kg m $^{-3}$) of the material, c is the specific heat capacity (J kg $^{-1}$K $^{-1}$), T is the current temperature, q is the vector of heat flux, Q is the rate of internal heat generation (W m $^{-3}$), tis the time (s), ∇is the spatial gradient operator and x, y, zare the coordinates in the reference plane. The non-liner isotropic Fourier heat flux constitutive equation given by Eq. (2) is employed.

$$q = -k\nabla T \quad \ldots\ldots(2)$$

Published By:
Blue Eyes Intelligence Engineering
and Sciences Publication (BEIESP)

Where k (W m $^{-1}$K $^{-1}$) is the temperature dependent thermal conductivityThe most widely acceptable double ellipsoidal heat source model, presented by Goldak et al. [18] as shown in Fig. 4, is used to present the heat generated by the welding torch for the heat input distribution tothe welds. The very small variations due to curvature of the cylinders are not taken into account. The model gives the Gaussian distribution for circumferential welding and has excellent features of power and density distribution control in the weld pool and HAZ. The spatial heat distribution in a moving frame of reference can be calculated with the governing equations Eq. (3) and Eq. (4) [18].

$$q_f = \frac{6\sqrt{3}\eta Q f_f}{\pi\sqrt{\pi} a_f bc} e^{\left\{-3\left(\frac{x^2}{a_f^2}+\frac{y^2}{b^2}+\frac{z^2}{c^2}\right)\right\}} \quad \text{.....(3)}$$

$$q_r = \frac{6\sqrt{3}\eta Q f_r}{\pi\sqrt{\pi} a_r bc} e^{\left\{-3\left(\frac{x^2}{a_r^2}+\frac{y^2}{b^2}+\frac{z^2}{c^2}\right)\right\}} \quad \text{.....(4)}$$

Where, **Q =VI** and $\mathbf{f_f + f_r = 2}$

$\mathbf{a_f}$ is the length of the front ellipsoidal (m) $\mathbf{a_r}$ is the length of rear ellipsoidal (m)**b** is the width of heat source (m) **c**is the depth of heat source (m) $\mathbf{f_f}$ is the fraction of heat in front ellipsoidal $\mathbf{f_r}$ is the fraction of heat in rear ellipsoidal **Q** is the total heat input (watts) **V** is the welding voltage (volts) **I** is the welding current (amperes)

III. EXPERIMENTAL VERIFICATION

The appropriate way to ensure the reliability of thenumerical simulations and to extend the utilization of the research work for shop floor applications is by conducting full-scale experiments with proper instrumentation for data measurement. For arc welding experiments, automatic welding setup with minimum human intervention and skill is considered as mandatory for the proper validation of numerical results due to the variations associated with the skill of the operators and rotary synchronization problems. Similarly, the careful data acquisition during the experiments is of critical importance and demands a proper data measurement and analysis system. In the present research, to ensure the reliability of the FE models, GTAW experiments on two thin-walled pipe with similar geometric and welding process parameters from the finite element models are conducted. Low carbon steel equivalent to AH36 with chemical composition as shown in Table 1 having slight variations in chemical composition from the material model used in the simulation is utilized. Similar approximations were made in the past by [22] with comparable measured and predicted results. In addition to the FE parameters, argon with 99.999% purity was used as shielding gas with flow rate of 15 liters/min. Commercially available high-tech, fully automatic SAF GTAW welding equipment along with rotary positioners and welding fixtures was used to reflect the desired structural boundary conditions. Single pass welding equipment along with rotary positioners and welding fixtures was used to reflect the desired structural boundary conditions. Single pass butt-weld geometry is used with single "V" groove having included angle of 90o and 2 mm root opening as shown in Fig. 4. The welding specimen consists of two 150 mm outer diameter and 3 mm wall thickness cylinders. Two tack welds starting from 0° (weld start position) equally spaced at 180°, each with length of ~ 8 mm were placed. These tack welds were also used to create a root opening prior to welding by insertion of additional spacers of 2 mm at some appropriate locations during tack welding.

Table 1. Chemical composition of low carbon steel. % Chemical Composition

%ChemicalComposition			
C	0.130	V	0.056
Cr	0.026	Cu	0.015
Mn	1.418	S	0.007
S	0.012	P	0.023
Si	0.346	Sn	0.002

The spacers were removed after the tack welds were cooled to room temperature. To minimize the initial stress effects prior to welding due to tack welds, the areas in and around the tack welds were treated with post weld heating to 573K (300°C). Conventional gas torch heating with both infrared and touch probe thermocouples measurement was utilized. However, the stress data after the tack welds and after the post weld heating was not recorded and the effects are ignored. Further, as these cylinders were linearly seam welded after roll forming of sheet metals, the effects of the linear seam weld was also not considered in this work. The furnace stress relieving prior to circumferential tack welds is a reasonable justification for not considering these effects. The nodal temperature distributions from the thermal analysis are used as a basic input for the sequel structural analysis. Therefore, experimental data correlation for the FZ and HAZ dimensions or alternatively some nodal temperature verification for accurate pre-dictions of subsequent stress fields and distortion patterns is a prerequisite. The latter technique by using the thermocouples and data acquisition system with computer interface is adopted for the thermal model validation in the present study. Thermocouples at four different locations were placed and temperature recorded through the data logger after every 10 seconds of time interval for comparison with FE results. A quantitative comparison of measured and predicted transient temperatures at thermocouple locations is presented in Fig. 5. The thermocouples TC1, TC2 and TC3 show close agreement with the FE data. Whereas, thermocouple TC4 shows comparatively higher variation of predicted and measured temperatures. Overall, the results are within the maximum variation of 8% and are reasonably accept-able. Residual stresses are measured at some specified points for comparison through the predicted results for structural model validation.

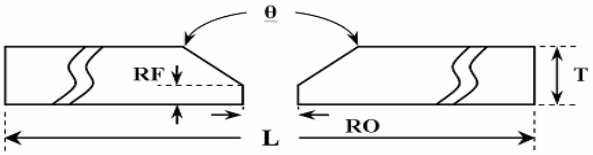

RF	θ	RO	T	L
1 mm	90°	2 mm	3 mm	300 mm

Fig. 4. Butt-weld joint geometry (not to scale).

Published By:
Blue Eyes Intelligence Engineering
and Sciences Publication (BEIESP)

A center hole drilling strain gauge method is used to measure the residual hoop and axial stresses at specified locations, i.e., points P1 to P3 on cylinder outer surface and P4 to P6 on cylinder inner surface. Refer to the gauge location from P1 to P6 in Fig. 6. The details of the hole drilling residual strain measurement method can be found in [20]. A quantitative comparison of residual stresses from experiments with predicted data, showing good agreement, can be found in Fig. 6. From the qualitative comparison of nodal temperatures and residual stresses from Fig. 5 and Fig. 6, it is evident that predicted results agreed well with the experimental data; thus the developed models have been experimentally validated.

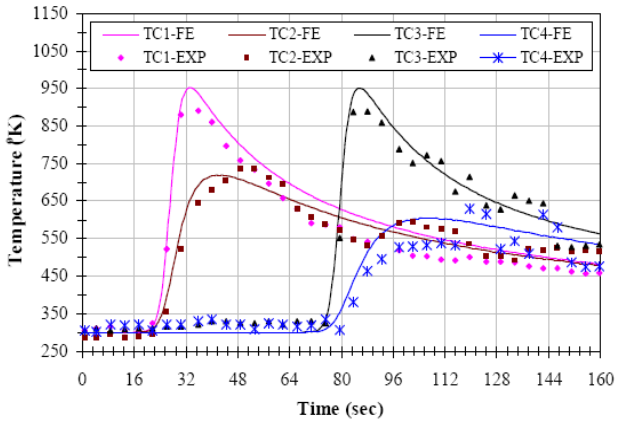

Thermocouplelocation	TC1	TC2	TC3	TC4
DistancefromW $_L$(mm)	10	15	10	20
Distancefromweldstart(^{0})	30	30	90	90

Fig. 5. Comparison of computed and measured transient temperature profiles at four different locations on pipe outer surface.

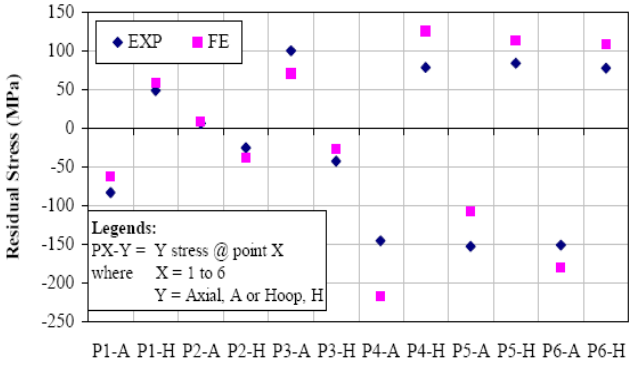

Pointreference(1to6)

Straingaugelocation	P1	P2	P3	P4	P5	P6
DistancefromW$_L$(mm)	10	15	20	10	10	10
Anglefromweldstart(^{0})	30	30	30	45	125	225

Fig. 6. Computed and measured residual stress values for different locations at pipeouter surface.

IV. ASPECTED RESULTS

4.1 Thermal analysis

Fig. 7(a-d) shows the temperature distributions for four different times during the welding process. As anticipated, the peak temperatures are observed at the heat source location (i.e., close to WL). Steep temperature gradients are observed ahead of the heat source, showing the least significance of heat flow ahead of the welding torch. The gradients behind the torch show the cooling phenomenon after peak temperature achieved, as the torch moves ahead from certain point. Fig. 7(d) shows the temperature distribution when the weldments are cooled to almost uniform temperature, followed by some more time steps further simulating the cooling phase.

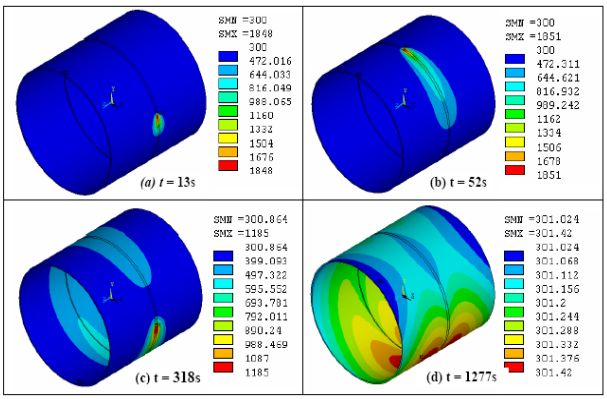

Fig. 7. Temperature profiles at four different time steps during the welding process.

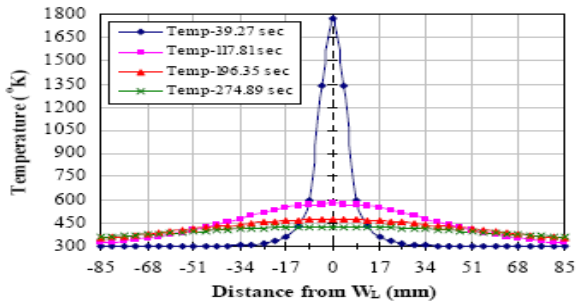

(a)

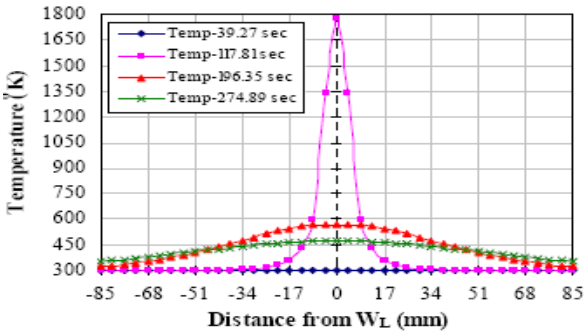

(b)

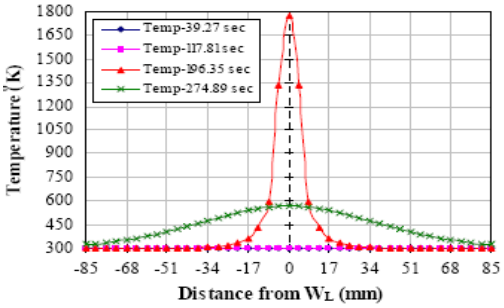

(c)

Published By:
Blue Eyes Intelligence Engineering and Sciences Publication (BEIESP)

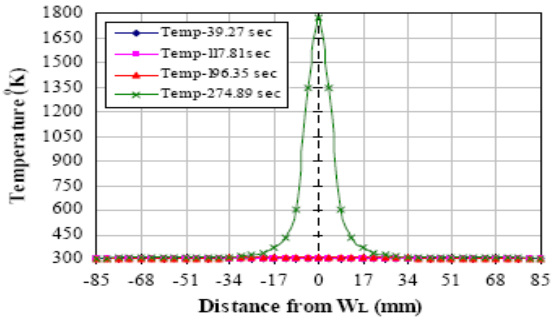

(d)

Fig. 8. Axial temperature distributions for four different cross-sections at different time steps from the weld start.

Fig. 8(a-d) shows the axial temperature distributions for different cross-sections at different time steps from the weld start towards the time progress. It is clear that the temperature distribution at a section is steep as the arc crosses the section, e.g., in case of Fig. 8(a) the section is located at an angle of 45° from the weld start position, i.e., 0°. A welding torch traveling at a speed of 3 mm/s around a circumference of 300 x πreaches the section after 39.27 s. Hence maximum temperature as expected is observed at the torch position. The temperature falls slowly as the torch crosses the section. A preheating action of the section due to the forward heat flow through the torch just before the torch arrival at a section is also shown and is more dominant incase for the sections oriented at 225° and 315°as depicted in Fig. 8(c) and Fig. 8(d), respectively. Fig. 9 further elaborates on the temperature distribution by using Goldak's heat source model.

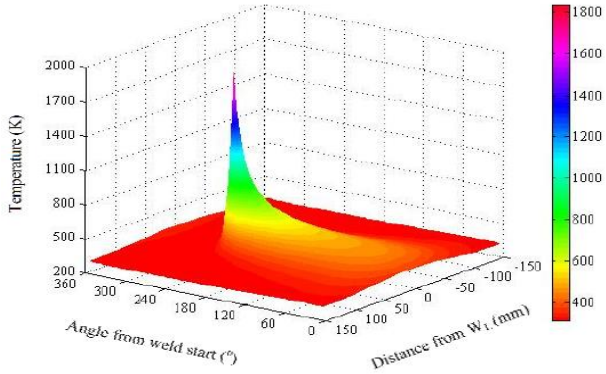

Fig. 9. Temperature contour plots.

4.2 Residual stress analysis 4.2.1 Axial residual stress fields

For circumferentially welded cylinders, stress normal to the direction of the weld bead is the axial stress. Compressive and tensile axial stress fields are observed in and near the weld region on the outer and inner surfaces of the cylinders, respectively. This is attributed to different temperature profiles on the inner and outer surfaces of the cylinders. Varying shrinkage patterns through the wall thickness on the inner and outer surfaces due to different temperature gradients; results in tensile and compressive residual stress fields on inner and outer surfaces, respectively, near the weld line (WL). Fig. 10 shows axial stress distributions on the cylinder's outer surface at different cross sections from the weld start position. The convention used is that Axial-50 represents the axial stress at 50° from the weld start position and so on.

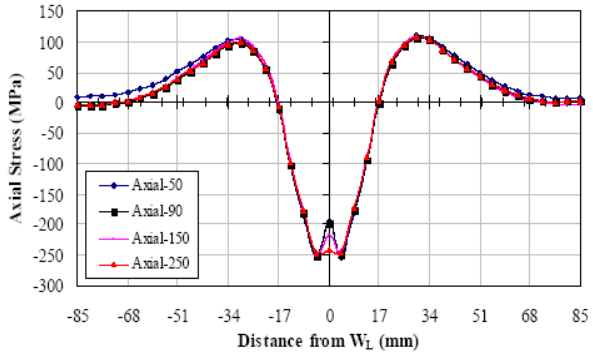

Fig.10. Residual axial stresses (MPa) on outer surface at different cross sections from the weld start position

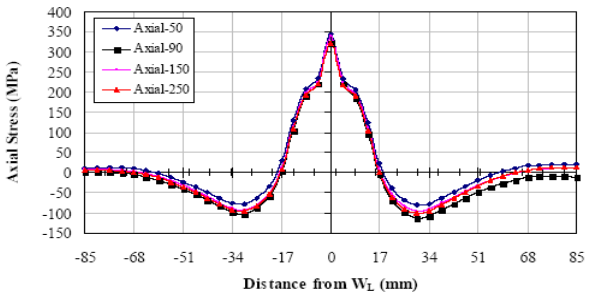

Fig. 11. Residual axial stresses (MPa) on inner surfaceat different cross sections from the weld start position.

The compressive residual axial stresses near the WL diminish to zero after 17 mm on both sides of the WL. Beyond this, a stress reversal from compressive to tensile is observed. These low magnitude tensile stresses again approach a zero value almost 68 mm away from the WL. After 68 mm from the WL a constant axial stress value near to zero is obvious from Fig. 10. The high tensile stresses near the WL approach to zero and then reverse to lower compressive residual stresses at 17 mm, again increasing to almost constant value of zero at 68 mm on both sides of WL observed for cylinder inner surfaces at different cross sections from weld start position as shown in Fig. 11.The general residual axial stress profile shows close analogy with the previous research [7, 10, 12, 14, 15]. The variation in magnitude (higher or lower residual stresses) in the present research work is attributed to the different material properties, i.e., mechanical properties like yield strength for base and weld filler metals along with other parameters such as weld geometry and heat source parameters. Some observations of the significance pertaining to axial stress fields from Fig. 10 and Fig. 11 are as follows:

• Due to symmetry across the WL, the stresses are also symmetric. In and around the FZ, the high magnitude stress fields, i.e., compressive and tensile for outer and inner surfaces, respectively, are observed.

• Axial stresses are weakly dependent on the circumferential location. Fig. 10 and Fig. 11 clearly reveal that axial residual stresses on outer and inner surfaces at four different cross sections (50°, 90°, 150° and 250°) are almost of the same magnitude and trend. This is in absolute agreement with the previous research [7]. Except the weld start and its vicinity, the axial stress around the circumferential direction almost has a homogeneous distribution.

Published By:
Blue Eyes Intelligence Engineering
and Sciences Publication (BEIESP)

• At the outer surface of cylinders near the WL, there is a prominent bulge indicating stress variations beneath the weld crown (refer Fig. 10).

4.2.2 Hoop residual stress fields.

Stresses parallel to the direction of the weld bead are known as hoop stresses. The residual hoop stresses are developed due to the radial expansion andcontraction during the heating and cooling sequence of welding process. Residual hoop stress distributions for outer and inner surfaces of cylinders along the axial directions in different cross sections from the weld start position are shown in Fig. 12 and Fig. 13, respectively. On the inner and outer surfaces, in and around the vicinity of the WL, large tensile and compressive hoop stresses, respectively, are developed. Similar trends for stress reduction and stress reversal are observed for hoop residual stresses as for axial residual stresses. The trend for the hoop stress also agreed well with the previous research [7, 10, 12, 14, 15]. The quantitative variation is again attributed to different welding parameters, heat source parameters and material properties in the present and referred research work, respectively. Some important aspects are as follows:

- Hoop residual stresses are also symmetric due to symmetry across the WL.
- Near the FZ high tensile stresses (130 MPa on outer and 313 MPa on inner surface) are predicted. Away from the HAZ region (about 17 mm from WL), both on outer and inner surfaces a compressive residual stress of 200 MPa is observed.
- Hoop stresses are dependent on the circumferential location from weld start to weld end. From Fig. 12 and Fig. 13 it is obvious that hoop residual stresses on outer and inner surfaces at three different cross sections (50°, 90°, and 250°) vary in magnitude, with almost similar trend. This is also in close agreement with the previous research [7].

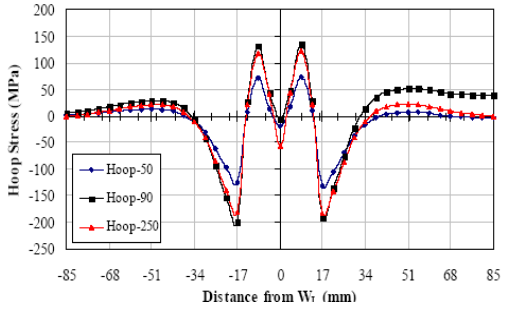

Fig.12. Residual hoop stresses (MPa) on outer surface at different cross sections from the weld start position

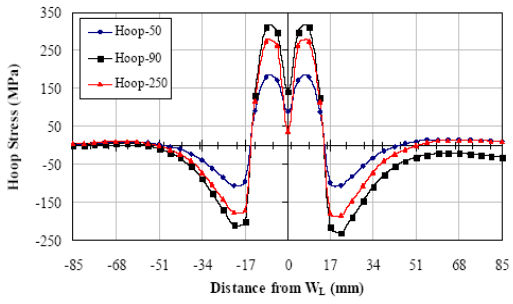

Fig.13. Residual hoop stresses (MPa) on inner surfaceat different cross sections from the weld start position

4.2.3 Axial and hoop residual stress fields along the circumference

Comparison of axial and hoop residual stress distribution for outer and inner surfaces, on a circumferential path at the WLis shown in Fig. 14. Again, the stress profiles are generally in agreement with the previous research. Some important observations are:

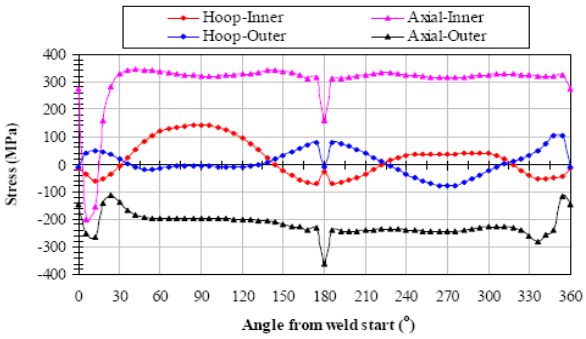

Fig. 14. Axial and hoop residual stress fields on pipe outer and inner surfaces on a circumferential path at the WL

• On the outer surface, the low magnitude hoop stress (-76 MPa to 77 MPa) remains almost constant. Some exceptions atweld start/end and tack weld locations (0° and 180°) are observed. At these locations, almost a zero hoop stress is observed. Slight variation in magnitude and trend is observed for hoop stresses on the inner surface. The stress varies from -70 MPa to 140 MPa, with some exceptions on weld start/end and tack weld locations. Again, at tack weld locations, stress values close to zero are observed.

• On the outer surface, a compressive axial stress profile is shown in Fig. 14. The compressive stress varies from 114 MPa to 361 MPa. A low magnitude, stable stress profile from weld start to weld end with some exceptions in and in vicinity of weld start/end and tack locations is observed. The significant effects of weld start are observed for axial stress on inner surface. Also at tack weld points, the effect is prominent. The stress varies from -200 MPa to about 340 MPa in magnitude. A dip of about 472 MPa and 150 MPa is shown at the weld start of 0° and tack weld locations of 180° respectively.

4.2.4 Stress contour plots

From previous discussion it is evident that due to weld start/end and tack welds, the residual stress varies significantly along the entire periphery. Fig. 10 and Fig. 11 for cylinder outer and inner surfaces, respectively, presents axial residual stresses at four different cross sections from weld start position at 0o. No presentable variation is observed because the data shown is away from the weld start/end and tack weld orientations. Similarly, slight variation in hoop residual stress patterns is observed from Fig. 12 and Fig. 13 for outer and inner surfaces, respectively. Again, the data at weld start/end and tack weld location(s) ismissing in this case. In order to get a better insight of the stress variation along the hoop co-ordinates, hoop residual stress fields on outer and inner surfaces are shown in Fig. 15 and Fig. 16, respectively.From Fig. 15, on outer surfaces the stress pattern on the whole periphery is strongly affected by the weld start/end and tack weld at 180°. Highly fluctuating stress patterns along the entire periphery, transverse to welddirection (axial direction) are obtained.

Published By:
Blue Eyes Intelligence Engineering
and Sciences Publication (BEIESP)

Pronounced localized stress reduction in and around the weld start/endand tack weld locations is shown.However, these effects are slightly less significant at the weld end location. Transverse to weld direction andaway from the weld line, stress reversal is shown along the entire periphery with some exceptions at weldstart/end and tack weld positions.Hoop residual stress fields from Fig. 16 on inner surface reveals that the effect

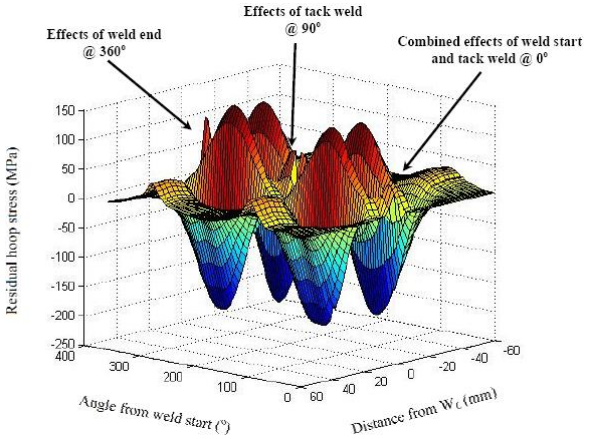

Fig. 15. Hoop residual stress fields on pipe outer surface.

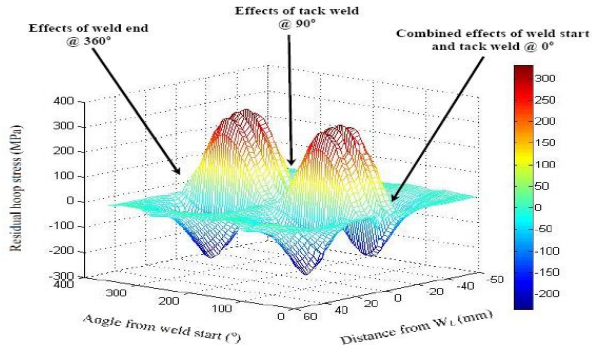

Fig. 16. Hoop residual stress fields on pipe inner surface.

of weld start and weld end are not as much pronounced as for the cylinder outer surface. However, the effects of tack weld location at 90° are quite significant. Over the entire periphery from weld start at 0° to weld end at 360°, hoop residual stress oscillates significantly in the transverse direction on both sides of the weld line. Away from the weld, the fluctuation trend is progressively stabilized.

4.3 Distortion analysis

4.3.1 Axial and radial deflection

Fig. 17 present the comparative (predicted and experimentally measured) axial tilt of the restraint-free face of the cylinder after the cooling of the weld-ments. Keeping in view the thickness of the cylinder face, it was difficult to accurately measure the face tilt of the cylinder experimentally. With some appropriate arrangements and welded cylinders still in the welding positioner, a digital dial indicator was precisely positioned at an average diameter of the cylinder (in this case 297 mm) and the data was recorded by rotating the positioner. To minimize the data acquisition error, five different readings after the tack weld and after cooling of the weld-ments to room temperature were taken. An average value is plotted in Fig. 17 for comparison with predicted results. Axial face tilt ranging from -0.34mm to +0.23mm is observed, as the dial indicator tracks the face from 0° to 360°. The extent of axial shrinkage is dependent on a number of factors including welding process parameters, tack weld dimensions and orientation.

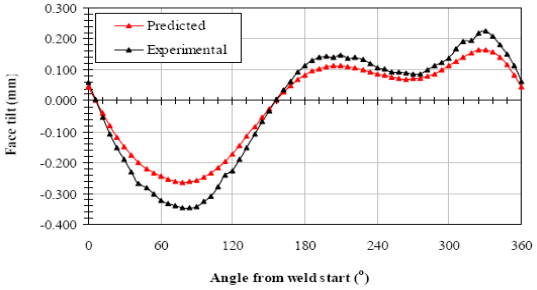

Fig. 17. Measured and predicted axial deformation (face tilt) sections from the of the cylinder face

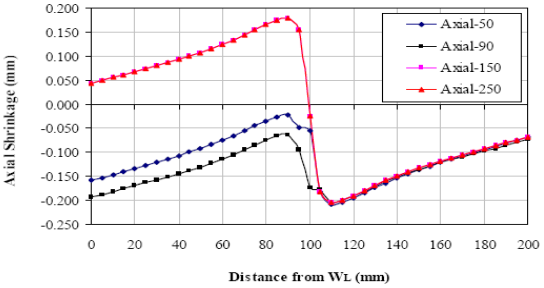

Fig.18. Axial shrinkage at four differentWL on pipe outer surface.

For the welding process parameters and tack weld geometry in the present research, the axial shrinkage is maximum (0.263 mm) at 78° and axial deflection is maximum (0.162 mm) at 330° near the weld end. From weld start position at 0º to 150º the FE results are under predicted as compared to experimental data, from 17% to 44% with an average under prediction of 24%. From 132º to 359º again low predicted results are observed with variation of 45% to 57% at an average under prediction of 45%. Although the variation is a bit on the larger side, the results are in good qualitative agreement from weld start to weld end. Fig. 18 shows the variability in axial shrinkage at four different sections from the WL, at cylinder outer surface. As the coordinate axis is located on the WL, the shrinkage on the restraint-free end is shown to be positive. Near the WL(10 mm from weld line towards free restraint free end), maximum axial shrinkage of 0.17 mm is indicated for axial sections at 50° and 150° from the weld start position. The axial shrinkage decreases away from the WLtowards the free end to a minimum value of 0.05 mm. Similarly, on the constrained end, a maximum axial shrinkage of 0.2 mm is observed at a distance of ~10 mm from WLfor all the sections under investigation. The axial shrinkage decreases continuously away from the WL and a minimum shrinkage of almost zero is shown at the restrained end.

V. CONCLUSIONS

Computational methodology and techniques based on finite element analysis for the prediction of temperature profiles and subsequent weld-induced residual stress fields and distortion patterns in GTA welded thin-walled pipe of low carbon steel are developed and implemented successfully with close correlation to the experimental investigations. Detailed results and discussion pertaining to residual stress fields are presented.

Published By:
Blue Eyes Intelligence Engineering and Sciences Publication (BEIESP)

Further, the author's also present some data pertaining to residual deformations.

The following are the significant conclusions from the results presented.

(1) In the girth-welded pipes, axial residual stresses in the weld vicinity are compressive in the outer surface and tensile in the inner surface. Hoop stresses aretensile in both inner and outer surfaces.

(2).Hoop residual stresses are sensitive to the angular location from the weld start position.

(3) Pipe wall thickness has a significant effect on the residual stress distributions in the girth-welded pipes. Thicker pipe tends to result in lower axial residual stresses, but higher hoop residual stresses.

(4) Maximum axial and radial deflection is observed near the weld line. The axial shrinkage decreases continuously away from the WL and a minimum shrinkage of almost zero shown at the restrained end. However, on the restraint free end some deflection (face tilt) is observed.

(5) On the inner surface, the weld start effect is more severe for both axial and hoop stresses and is dominant in the weld start direction. A significant effect of tacks on the axial stress on the inner surface is observed at angular positions of 0° and 180° from the weld start point, whereas the effect of tacks on hoop stresses is not as prominent. The author has concluded that the stress distribution is no more axis-symmetric for a single pass butt circumferential weld with initial tacks. However, if the weld start/end effects are ignored, hoop stresses are almost uniform.

REFERENCES

1. Rybicki, E. F., Schmueser, D. W., Stone-sifer, R. W., Groom, J. J., Mishler, H. W. 1978. A finite-element model for residual stresses and deflections in girth-butt welded pipes. Journal of Pressure Vessel Technology, Vol. 100, pp. 256-262.
2. Brust, F. W., Stonesifer, R. B. 1981. Effect of weldingarameters on residual stresses in BWR piping systems. EPRI NP-1743, Project 1174-1, Final Report
3. Karlsson, C. T. 1989. Finite element analysis of temperatures and stresses in a single-pass butt-welded pipe-influence of mesh density and material modeling. Engineering Computations, Vol. 6, pp. 133-141..
4. Fujita, Y., Nomoto, 1., Hasegawa, H. 1980. Deformations and residual stresses in butt welded pipes and shells. Nav. Archit. a.OceanEngng. (Soc. of Nay. Archit. of Jap.) 18, pp. 164-174, and IIW-Doc. X-963-80
5. Josefson, B. L. 1983. Stress redistribution [12] Y. Dong, J. Hong, C. Tsai and P. Dong. Finite Element modeling of residual stresses in austenitic stainless steel pipe girth welds, Welding Journal, Weld Research Supplement,442 (1997) 449-444.
6. A. Yaghia, T. H. Hydea, A. A. Becker, W. Suna and J. A. Williams, Residual stress simulation in thin and thick-walled stainless steel pipe welds including pipe diameter effects, International Journal of Pres-sure Vessels and Piping,83 (11-12) (2006) 864-874.
7. D. Deng and H. Murakawa, Numerical simulation of temperature field and residual stress in multi-pass welds in stainless steel pipe and comparison with experimental measurements, Computational Material Science,37 (3) (2006) 269-277
8. B. Brickstad and B. L. Josefson, A parametric study of residual stresses in multi-pass butt-welded stainless steel pipes, International Journal of Pres-sure Vessels and Piping,75 (1) (1998) 11-25.
9. E. F. Rybicki, D. W. Schmueser, R. W. Stonesifer, J. J. Groom and H. W. Mishaler, A Finite Element model for residual stresses and deflections in girth-butt welded pipes, ASME Journal of Pressure Ves-sel Technology,100 (1978) 256-262.
10. E. F. Rybicki, P. A. McGuire, E. Merrick and J. Wert, The effect of Pipe thickness on residual stresses due to girth welds. ASME Journal of Pres-sure Vessel Technology, 104 (1982) 204-209
11. E. F. Rybicki and R. B. Stonesifer, Computation ofresidual stresses due to multi-pass welds in piping system. ASME Journal of Pressure Vessel Technology, 101 (1979) 49-54.
12. Y. Dong, J. Hong, C. Tsai and P. Dong. Finite Element modeling of residual stresses in austenitic stainless steel pipe girth welds, Welding Journal, Weld Research Supplement,442 (1997) 449-444.
13. R. I. Karlsson and B. L. Josefson, Three- dimensional Finite Element analysis of temperature and stresses in single-pass butt-welded pipe. ASME Journal of Pressure Vessel Technology,112 (1990) 76-84.
14. M. Jonsson and B. L. Josefson, Experimentally determined transient and residual stresses in the butt-welded pipes, Journal of Strain Analysis,23 (1) (1988) 25-31.
15. L. Karlsson, M. Jonsson, L. E. Lindgren, M. Näss-tröm and L. Troive, Residual stresses and deforma-tions in a welded thin-walled pipe, Proc. ASME Pressure Vessel and Piping Conf. (Hawaii, July 1989)PVP-173 (1989) 7-11.
16. S. Fricke, E. Keim and J. Schmidt, Numerical weld modeling-a method for calculating weld-induced residual stresses, Nuclear Engineering and Design,206 (2-3) (2001) 139-150.
17. ANSYS-10.0 user manual.
18. J. Goldak, A. Chakravarti and M. Bibby, A new Finite Element model for welding heat source. Metallurgical Transactions B. 15B (1984) 299-305
19. L. F. Anderson, Residual stresses and deformations in steel structures, PhD. Thesis, Technical University of Denmark,(2000)
20. Vishay Group, Measurement of residual stresses by the hole drilling strain gage method, Technical Note No.TN-503. (www.vishay.com/brands/measurements_group/guide/tn/tn503/503index.htm).
21. P.J. Bouchard, D. George, J.R. Santisteban, G. Bruno, M. Dutta, L. Edwards, E. Kingston,D.J. Smith, Measurement of the residual stresses in a stainless steel pipe girth weld containing long and short repairs, International Journal of Pressure Vessels and Piping, 82,(4), (2005),299–310
22. W.C. Jiang,B.Y. Wang,J.M. Gong,S.T. Tu, Finite element analysis of the effect of welding heat input and layer number on residual stress in repair welds for a stainless steel clad plate, Materials & Design, 32(5), (2011), 2851–2857
23. Chin-Hyung Lee, Jeong-HoonBaek, Kyong-Ho Chang, Bending capacity of girth-welded circular steel tubes, Journal of Constructional Steel Research,75 (2012), 142–151
24. Chin-Hyung Lee, Kyong-Ho Chang, Jeong-Ung Park, Three-dimensional finite element analysis of residual stresses in dissimilar steel pipe welds, Nuclear Engineering and Design256, (2013),160–168

AUTHOR PROFILE

Prabhat Kumar Sinhais a M.Tech in CAD. He is having overall 6 year of teaching experience.His major interests are in Auto Mobile Engg., Principles of Machine Design,FEM, Foundry Technology, Industrial Engg. Mgt.Published various papers in international journals.

Raisul Islam is a M.Tech(Production & Industrial Engineering) Pursuing from SHIATS,Alld-211007. He is having overall 2 year of teaching experience.His major interests are in Manufacturing Science,ProductionEngg., Fabrication.

Chandan Prasad : M.tech(Production & Industrial Engineering) PursuingFrom SHIATS,Alld-211007 His major interests are in design, manufacturingScience, Industrial Relation. Published a papers in (IJMET).

Mohd. kaleem :M.tech(Production & Industrial Engineering) PursuingFrom Sam Higginbottom Institute of Agriculture Technology and sciences,Allahabad 211007

Published By:
Blue Eyes Intelligence Engineering and Sciences Publication (BEIESP)